HHS Public Access

Author manuscript

Eur Radiol. Author manuscript; available in PMC 2024 August 01.

Published in final edited form as:

Eur Radiol. 2023 August ; 33(8): 5321–5330. doi:10.1007/s00330-023-09545-9.

The Technical Development of Photon Counting Detector CT

Cynthia H. McCollough, Ph.D.[1], **Kishore Rajendran, Ph.D.**[1], **Shuai Leng, Ph.D.**[1], **Lifeng Yu, Ph.D.**[1], **Joel G. Fletcher, M.D.**[1], **Karl Stierstorfer, Ph.D.**[2], **Thomas G. Flohr, Ph.D.**[2]

[1]Department of Radiology, Mayo Clinic, Rochester, MN USA

[2]Siemens Healthineers, Forchheim, Germany

Abstract

Since 1971 and Hounsfield's first CT system, clinical CT systems have used scintillating energy-integrating detectors (EIDs) that use a two-step detection process. First, the x-ray energy is converted into visible light and second, the visible light is converted to electronic signals. An alternative, one-step, direct x-ray conversion process using energy resolving, photon-counting detectors (PCDs) has been studied in detail and early clinical benefits reported using investigational PCD-CT systems. Subsequently, the first clinical PCD-CT system was commercially introduced in 2021. Relative to EIDs, PCDs offer better spatial resolution, higher contrast-to-noise ratio, elimination of electronic noise, improved dose efficiency, and routine multi-energy imaging. In this review article, we provide a technical introduction to the use of PCDs for CT imaging and describe their benefits, limitations, and potential technical improvements. We discuss different implementations of PCD-CT ranging from small-animal systems to whole-body clinical scanners and summarize the imaging benefits of PCDs reported using preclinical and clinical systems.

Keywords

Tomography; X-Ray Computed; Radiation Dosage; Humans; Photons; Iodine

Introduction to energy resolving, photon counting detector technology

Energy resolving, photon-counting detectors (PCDs) have only recently been used in medical CT [1–3]. The typical setup of such a is shown in Fig. 1. At the heart of the detector is a semiconductor layer made of cadmium-telluride (CdTe), cadmium-zinc-telluride (CZT), or silicon. After passing through the patient, the X-rays are absorbed in this layer and generate charge clouds that are separated in the strong electric field created by a high voltage (800–1000 V) between the cathode on the top and pixelated anode electrodes at the bottom of the detector. The electrons move to the anodes and induce short current pulses. A pulse shaping circuit converts the current pulses into voltage pulses with a width at half the maximum signal of 10–15 ns. The amplitude of the voltage pulses is proportional to the absorbed energy. When the pulse height exceeds a threshold, the pulse is counted

Corresponding Author: Cynthia H. McCollough, PhD, 200 First Street SW, Rochester, MN 55905, Phone: (507) 538-0633, Fax: (507) 266-3661, mccollough.cynthia@mayo.edu.

by electronics. A PCD can also be operated with multiple voltage thresholds to provide energy-resolved data.

Energy resolving, PCDs have several advantages over the solid-state scintillating detectors used in medical CT systems today. In scintillating detectors, the energy of the X-ray photon is first converted into visible light, which then generates an electric current. The individual detector elements must be separated by reflective septa to prevent optical crosstalk. These layers reduce the geometric dose efficiency of the detector because the X-ray quanta absorbed in them do not contribute to the measured signal. To keep the loss caused by these dead zones at an acceptable level, the active detector elements cannot become smaller and smaller, which ultimately limits the achievable spatial resolution that can be achieved with scintillating detectors. Energy resolving, PCDs, on the other hand, do not require these septa between the individual pixels and can therefore be made much smaller. The geometric dose efficiency is only reduced by the anti-scatter grids, which are necessary for all forms of CT detectors. The anti-scatter grids do not have to be placed between each individual detector element when the detector pixels are very small (e.g., < 0.2 mm when projected onto the isocentre). Thus, PCDs can achieve resolutions of up to 40 lp/cm, in contrast to the maximum of 20 lp/cm with scintillating detectors [4]. Higher spatial resolution provides significant clinical benefits for CT examinations of bony structures, lungs, and small vessels provided that any increase in noise is adequately addressed. These benefits are described in the second part of this review [5].

In energy resolving PCDs, all pulses produced by absorbed X-rays are counted as soon as they exceed a threshold voltage that is representative of a photon energy T_0, the value of which typically corresponds to approximately 20–25 keV. Electronic noise has a very low amplitude and is well below this threshold. Hence, electronic noise does not result in counts and even at very low doses, statistical Poisson noise is the dominant source of noise. CT scans at very low radiation doses or CT scans of obese patients therefore have lower image noise, less streak artifacts, and more stable CT-numbers than the corresponding scans with a scintillating detector, and radiation dose reduction beyond today's limits seems possible [6; 7].

Because they are simply counted, all X-ray quanta contribute with equal weight to the detector signal regardless of their energy E. There is no down-weighting of lower-energy X-ray quanta as in scintillating detectors. Low-energy quanta essentially determine the contrasts between different tissues in a CT image. In scans with iodine contrast agent, whose absorption is particularly large just above its K-edge of 33 keV, PCDs produce CT images with better iodine contrast-to-noise ratio [8]. This can be translated into either a reduction of radiation dose or of the amount of contrast agent.

Energy resolving PCDs can be operated using multiple threshold energies. Fig. 2 illustrates the simultaneous acquisition of four measurement signals S_0, S_1, S_2 and S_3 in which the energy of the detected quanta exceeds the thresholds T_0, T_1, T_2 and T_3, respectively. Subtracting detector signals with adjacent energy thresholds produces "energy bin" data that contain all X-ray counts with energies between the two thresholds. Energy-resolved measurement of CT data enables multi-energy material differentiation in any CT scan. All

established dual energy applications are feasible with two energy bins [9]. Data acquisition with three and more bins enables differentiation of two contrast agents (iodine and another material with a K-edge > 40 keV, e.g., gadolinium or gold) [10; 11].

Physical limitations of PCDs

Detectors made of materials with low atomic number Z (e.g., silicon) suffer decreased photo-electric absorption and an increased amount of Compton scattering within the detector compared to detectors made of high Z materials. X-rays that are Compton scattered in the detector lose information about the original interaction location, resulting in a loss of sharpness in the resulting image. Some of the scattered photons also leave the detector without contributing to the measured signal, resulting in lower dose efficiency.

For high Z detectors (e.g., CdTe or CZT), there is little Compton scattering in the detector and most photons are absorbed directly via the photoelectric effect. However, there are two effects that result in information loss: First, the photoelectric effect results in an electron being ejected from an inner electron shell (typically K shell) of atoms of the detector material. When the electron vacancy is filled, characteristic photons may be emitted from the atoms, which can carry some of the incident energy out of the detector pixel. This is referred to as K-escape. Second, if the absorption of the incident X-ray photon occurred close to the pixel boundary, the resulting charge cloud may be split between two adjacent pixels. This is referred to as charge sharing. As a result, a single high-energy X-ray photon may be incorrectly counted as multiple lower energy photons. For example, an 80 keV photon may appear as a 50 keV photon in one pixel and a 30 keV photon in the next. This causes a significant distortion of the measured x-ray spectrum that affects multi-energy applications.

With larger pixels, the relative contribution of charge sharing and K-escape to the detector signal is smaller, but pulse pile-up becomes more relevant. At high X-ray flux (CT systems typically produce up to 10^9 photons/s/mm^2 in areas of low attenuation), X-rays can hit a detector pixel too quickly to be registered separately. Multiple overlapping pulses are counted as one photon interaction at too high of an energy. This is referred to as pulse pile-up. Pulse pile-up can lead to nonlinear count rates and eventually to saturation of the detector [12]. One approach to reducing pulse pile-up is to use smaller detector pixels, although the effects of k-escape and charge sharing will consequently increase. Another approach is to use Si-based PCDs in edge-on geometry as they have a higher charge carrier mobility and can handle higher x-ray fluxes without suffering from pulse pile-up [13].

Challenges to realization of clinical PCD-CT

High-yield fabrication of detector materials (e.g., CdTe, CZT, Si)

A good overview of the progress in CdTe and CZT crystal growth technology can be found in [14]. CdTe as a detector material has been studied since the 1950s [15]. The growth of high resistivity crystals is a complex challenge [16; 17]. The main breakthrough came with the usage of the traveling heater method by Acrorad for CdTe and Redlen for CZT [14; 18]. Due to its advantages, particularly for CdTe or CZT crystal growth, the traveling

heater method is now the method of choice for the high-yield production of these materials. However, it is still a complicated technology and growth rates are rather slow [18].

High speed application specific integrated circuits (ASICs)

A 2016 overview of ASICs used for the readout of direct converting semiconductors can be found in [19]. There is an interesting trade-off governing the choice of a pixel size: using a small pixel size will allow higher photon fluxes to be processed since a single pixel will see less photons per time. This minimizes pulse pile-up. Another advantage of smaller pixels is that smaller pixels will lead to shorter pulses which additionally increases the high-flux capabilities of the detector. This is the so-called small pixel effect [19]. On the other hand, small pixel sizes will increase the amount of charge sharing and k-escape, distorting the spectral response. The main challenge in developing a readout ASIC is navigating the contradicting requirements to keep both the electronic noise and the power consumption as low as possible.

PCD development and early systems

Benchtop and small animal systems

Early evaluations of PCDs were performed using small-animal scanners and benchtop systems. Preclinical studies were reported using investigational systems equipped with silicon, CdTe, CZT and gallium-arsenide PCDs with two to eight energy bins and detector pixel sizes as small as 55-μm to provide early insights into the clinical potential of this detector technology [20–25]. For example, small-animal studies using mice and rabbit models were performed using these systems to investigate material-specific imaging of vulnerable atherosclerotic plaques using gold nanoparticles [23] and tumour differentiation based on enhanced permeability and retention of liposomal iodine [20]. These systems also facilitated scanning of *ex vivo* human tissues, such as arterial segments with atherosclerotic plaques [26] or contrast-enhanced cartilage specimens [27; 28]. Further, physical concepts such as spectral distortion, charge sharing, and pulse pile up effects were evaluated using bench-top systems.

Pre-clinical systems

GE system—A full field-of-view prototype PCD-CT scanner was developed by GE Healthcare using CdTe PCDs developed by DxRay to replace conventional EID on a GE VCT scanner [29–31]. The detector had 2 energy bins and a rather limited count rate capacity of 5×10^6 counts/s/mm^2. The detector pixel was 1×1 mm^2 and configured in a 2D multi-slice geometry, with 1000 × 32 detector pixels (32-slice CT system). The system was later installed at Rabin Medical Centre in Israel and a few human subject scans were performed, including a carotid angiography and an abdominal exam, using relatively lower tube current (e.g., 140 mA, 140 kV, 1 s rotation for the abdominal scan) than that used in routine clinical exams [30]. Various types of dual-energy images were generated from the PCD-CT scanner, including virtual monoenergetic images, iodine maps, atomic number (z) maps, and virtual non-contrast images [29–32]. A full-sized CT system using deep edge-on arrays of Si based detectors has been built by GE and at the time of this writing, is undergoing early patient studies.

Siemens systems—A whole-body research PCD-CT system (SOMATOM CounT) was built by Siemens Healthineers using their second generation dual-source CT system (SOMATOM Definition Flash), with one of the two detector arrays replaced with a CdTe PCD [7; 33–37]. The PCD array has 32 rows of 0.9 mm x 0.9 mm detector macro pixels, corresponding to 0.5 mm by 0.5 mm at the iso-centre. Each macro pixel contains 4×4 square sub-pixels of size 0.225×0.225 mm^2. Data can be obtained using either the maacro pixel (4×4 sub-pixels) or in an ultra-high-resolution (UHR) mode (2×2 sub-pixels), which has an effective detector size of 0.25×0.25 mm^2 at the iso-centre. Each detector configuration has 2 energy thresholds, with 4 energy thresholds available using a special “chess” mode [36], which operates every other macro pixel at a different energy threshold, creating a chess board like distribution of the four energy thresholds. The field of view (FOV) of the PCD array is 275 mm while the FOV of the EID system is 500 mm. For objects larger than the 275 mm, a low dose data completion scan was required to avoid truncation artifacts [7]. An important feature of this system is that it allows high fluxes with a tube current up to 550 mA, which is sufficient for most whole-body scans and comparable to the tube current provided by commercial EID-CT scanners [7]. Units were installed at three medical centres (Mayo Clinic, NIH, and German Cancer Centre) and extensive patient studies have been performed on these systems, demonstrating various benefits of PCD-CT compared to EID-CT, including improved spatial resolution (150 um), lower radiation dose, reduced image artifacts, and simultaneous high-resolution, multi-energy imaging [2; 4; 6; 9; 11; 38–40].

Later, a single-source PCD-CT research system (SOMATOM CounT Plus) was built by Siemens Healthcare with a full 500 mm FOV on the PCD array [41]. The system has 2 scan modes: multi-energy mode with 144 × 0.4 mm (57.6 mm) collimation and 2 energy thresholds, or a UHR mode with 120 × 0.2 mm collimation and 1 energy threshold. This FOV and z-axis coverage are comparable to that of commercial EID scanners and no data completion scan is required. The PCD array consists of 0.275 × 0.322 mm^2 sub-pixels, which corresponds to 0.151 × 0.176 mm^2 at isocentre [1; 41]. With the presence of collimator blades, the effective minimum reconstructed slice width is 0.2 mm for the UHR mode and 0.4 mm for the multi-energy mode. A similar detector configuration is used in the commercial dual-source PCD-CT (NAEOTOM Alpha) by the same manufacturer [42].

Philips system—A prototype spectral photon counting CT (SPCCT) system was built by Philips and installed at Hospices Civils de Lyon in France [43]. The system was built upon one of the manufacturer’s EID platforms (iCT) using a 2-mm-thick CZT PCD and ChromAIX2 ASIC. Each pixel has 5 energy thresholds with a detector pitch of 0.274 × 0.274 mm^2 at isocentre in the high-resolution mode. The system has a full 50 cm FOV and 64×0.275 mm (17.6 mm) z coverage. Patient studies have been performed using the system to investigate clinical benefits in various areas such as cardiac and lung imaging [44; 45].

Early evidence of the benefits of PCD-CT

Absence of electronic noise

In low dose exams, electronic noise from EIDs translate to streak artifacts and CT number instabilities in the reconstructed images. The presence of electronic noise and associated artifacts limit the extent of dose reduction that can be achieved using EID-CT systems for low-dose exams such as lung cancer screening. The influence of electronic noise can be eliminated in PCDs via energy thresholding [12]. When the lowest energy threshold is set to be above the low-magnitude electronic noise level, true x-ray counts can be separated from electronic noise (Fig. 2, top), consequently resulting in fewer artifacts and improved CT number stability at lower radiation doses (Fig. 3) [6].

Increased image contrast

Low energy x-rays (e.g., <40–50 keV) carry significant tissue contrast information, particularly from iodine and bone. However, at these lower energies, EIDs produce lower signal values compared to at higher-energy x-rays. Unfortunately, the higher energy photons carry little to no tissue contrast information but produce the most signal. Since PCDs count each photon and assign them to individual energy bins, all photons are weighted equally, irrespective of their energy. Consequently, lower energy photons make a greater contribution to PCDs relative to EIDs, resulting in improved image contrast and contrast-to-noise ratio (Fig. 4). In addition to this fundamental advantage, since x-rays are binned based on their energies, user-defined weights can be assigned to individual energy bins post acquisition to potentially enhance image contrast [46].

Smaller detector pixels

Optical reflectors between EID pixels mitigate optical crosstalk between neighbouring pixels. The finite-sized interpixel reflectors result in dead zones between EID pixels; this leads to geometric dose inefficiency. Since no visible light is created in PCDs, interpixel septae are not required. Consequently, very small detector pixels (e.g., 150 μm at isocentre [1; 41]) can be used without sacrificing geometric dose efficiency. Several reports in the literature have demonstrated the clinical benefits of increased spatial resolution from PCD-CT. In addition to higher spatial resolution, the finer detector sampling from smaller PCD pixels can be leveraged to reduce image noise [47]. When data are acquired with a PCD array with finer detector sampling, lower image noise can be achieved when the CT image [4] is reconstructed with an image sharpness (i.e., reconstruction kernel) smoother than the maximum spatial resolution of the system (Fig. 5). Alternatively, the noise reduction benefit can be leveraged to achieve a radiation dose reduction at a fixed target image noise.

The increased spatial resolution of PCDs requires use of smaller image voxels to adequately convey the improved resolution. As shown in Fig. 5, this can be accomplished for similar noise and dose levels relative to EID-CT. However, for very high spatial resolution images (e.g., 0.2–0.25 mm isotropic resolution), increased noise is observed and hence measures to control image noise, such as iterative reconstruction or deep learning denoising, are needed.

Simultaneous multi-energy imaging

Since each detector pixel of a PCD-CT system is equipped with dedicated electronics to count and bin x-ray photons according to their respective energies, multi-energy (spectral) data are inherently acquired at constant tube potential. This is a fundamental advantage over traditional dual-energy CT based on dual-source or rapid tube potential switching, where two different tube spectra are required to capture spectral CT data. Therefore, PCD-CT enables high-resolution, spectral acquisitions at a single tube potential for all exam types. This allows for routine generation of virtual monoenergetic images, virtual non-calcium or non-contrast images and iodine maps.

Future Technical Directions

Coincidence counting

An ideal PCD would register each photon with its true energy at the original impact location. Physical mechanisms such as charge sharing and K-escape, however, lead to a spread of energy from the original impact location to adjacent detector pixels [48; 49]. Schemes have been proposed to sum signals arriving simultaneously in neighbouring pixels, attributing the sum of the signals to the pixel with the largest contribution. This “charge summing” scheme has been implemented in the Medipix3 prototype detector [50; 51]. The main drawback of this approach is that the method requires extensive analogue pixel-to-pixel communication which substantially increases the dead time, making it too slow for high-flux applications like CT.

An alternative approach pioneered by Hsieh [52; 53] would require registering counts occurring simultaneously in neighbouring pixels. The main simplification of this “coincidence counting” scheme is that it would not require any analogue communication between the pixels, hence avoiding an increase of dead time or pileup. The counts registered in these additional coincidence counters can be used to correct the counts distorted by charge sharing or K escape. In its simplest form, two counts in a low bin in two neighbouring pixels would be replaced by one count in the upper energy bin in one of the pixels. The method works providing that the count rate is not so high as to cause two or more near-simultaneous counts in adjacent detectors to be mistaken for one “charge shared” count. The resulting improvement in the spectral response is demonstrated in Fig. 6. This simple mechanism succeeds both in removing the low bin double counting peak between 40 and 65 keV and in substantially reducing the number of high energy photons that are registered in the lower energy bin.

Summary and conclusions

PCD-CT offers numerous technical advantages over conventional EID-CT systems, due to its fundamentally different approach to x-ray detection. The promising early investigations into energy-resolving PCDs have led to the culmination of clinical PCD-CT systems, with higher spatial resolution, improved contrast-to-noise ratio, improved radiation dose efficiency, and the routine availability of multi-energy capabilities as notable technical

features that can substantially enhance diagnostic CT. The advent of PCD-CT has also led to early investigations into multi-contrast imaging and functional imaging using nanoparticles.

Abbreviations:

PCD	photon counting detector
EID	energy integrating detector
CdTe	cadmium telluride
CZT	cadmium zinc telluride
ASIC	application specific integrated circuits
UHR	ultra-high resolution
FOV	field of view

References:

1. Flohr T, Petersilka M, Henning A, Ulzheimer S, Ferda J, Schmidt B (2020) Photon-counting CT review. Phys Med 79:126–136 [PubMed: 33249223]
2. Leng S, Bruesewitz M, Tao S et al. (2019) Photon-counting Detector CT: System Design and Clinical Applications of an Emerging Technology. Radiographics 39:729–743 [PubMed: 31059394]
3. Willemink MJ, Persson M, Pourmorteza A, Pelc NJ, Fleischmann D (2018) Photon-counting CT: Technical Principles and Clinical Prospects. Radiology 289:293–312 [PubMed: 30179101]
4. Leng S, Rajendran K, Gong H et al. (2018) 150-μm Spatial Resolution Using Photon-Counting Detector Computed Tomography Technology: Technical Performance and First Patient Images. Invest Radiol 53:655–662 [PubMed: 29847412]
5. McCollough C, Rajendran K, Baffour F et al. (2022) Clinical applications of photon counting detector CT. Eur Radiol (In Press)
6. Symons R, Cork TE, Sahbaee P et al. (2017) Low-dose lung cancer screening with photon-counting CT: a feasibility study. Phys Med Biol 62:202–213 [PubMed: 27991453]
7. Yu Z, Leng S, Kappler S et al. (2016) Noise performance of low-dose CT: comparison between an energy integrating detector and a photon counting detector using a whole-body research photon counting CT scanner. J Med Imaging 3:043503
8. Gutjahr R, Halaweish AF, Yu Z et al. (2016) Human Imaging With Photon Counting-Based Computed Tomography at Clinical Dose Levels: Contrast-to-Noise Ratio and Cadaver Studies. Invest Radiol 51:421–429 [PubMed: 26818529]
9. Leng S, Zhou W, Yu Z et al. (2017) Spectral performance of a whole-body research photon counting detector CT: quantitative accuracy in derived image sets. Phys Med Biol 62:7216–7232 [PubMed: 28726669]
10. Muenzel D, Daerr H, Proksa R et al. (2017) Simultaneous dual-contrast multi-phase liver imaging using spectral photon-counting computed tomography: a proof-of-concept study. Eur Radiol Exp 1:25 [PubMed: 29708205]
11. Symons R, Krauss B, Sahbaee P et al. (2017) Photon-counting CT for simultaneous imaging of multiple contrast agents in the abdomen: An in vivo study. Med Phys 44:5120–5127 [PubMed: 28444761]
12. Danielsson M, Persson M, Sjölin M (2021) Photon-counting x-ray detectors for CT. Phys Med Biol 66:03tr01
13. Persson M, Huber B, Karlsson S et al. (2014) Energy-resolved CT imaging with a photon-counting silicon-strip detector. Phys Med Biol 59:6709–6727 [PubMed: 25327497]

14. Fiederle M, Procz S, Hamann E, Fauler A, Frojdh C (2020) Overview of GaAs und CdTe Pixel Detectors Using Medipix Electronics. Crystal Research and Technology 55:2000021
15. Kröger FA, De Nobel D (1955) XXIV. Preparation and Electrical Properties of CdTe Single Crystals. Journal of Electronics and Control 1:190–202
16. Fougeres P, Siffert P, Hageali M, Koebel JM, Regal R (1999) CdTe and Cd1-xZnxTe for nuclear detectors: facts and fictions. Nuclear Instruments & Methods in Physics Research Section A-Accelerators Spectrometers Detectors and Associated Equipment 428:38–44
17. Szeles C, Eissler EE (1997) Current Issues of High-Pressure Bridgman Growth of Semi-Insulating CdZnTe. MRS Proceedings 487:3
18. Triboulet R (2015) Crystal Growth by Traveling Heater Method. In: Rudolph P, (ed) Handbook of Crystal Growth. Elsevier, Boston, pp 459–504
19. Ballabriga R, Alozy J, Campbell M et al. (2016) Review of hybrid pixel detector readout ASICs for spectroscopic X-ray imaging. Journal of Instrumentation 11:P01007–P01007
20. Badea CT, Clark DP, Holbrook M, Srivastava M, Mowery Y, Ghaghada KB (2019) Functional imaging of tumor vasculature using iodine and gadolinium-based nanoparticle contrast agents: a comparison of spectral micro-CT using energy integrating and photon counting detectors. Phys Med Biol 64:065007 [PubMed: 30708357]
21. Bennett JR, Opie AM, Xu Q et al. (2014) Hybrid spectral micro-CT: system design, implementation, and preliminary results. IEEE Trans Biomed Eng 61:246–253 [PubMed: 23996533]
22. Clark DP, Holbrook M, Lee CL, Badea CT (2019) Photon-counting cine-cardiac CT in the mouse. PLoS One 14:e0218417 [PubMed: 31536493]
23. Cormode DP, Roessl E, Thran A et al. (2010) Atherosclerotic plaque composition: analysis with multicolor CT and targeted gold nanoparticles. Radiology 256:774–782 [PubMed: 20668118]
24. Ronaldson JP, Zainon R, Scott NJ et al. (2012) Toward quantifying the composition of soft tissues by spectral CT with Medipix3. Med Phys 39:6847–6857 [PubMed: 23127077]
25. Scholz J, Birnbacher L, Petrich C et al. (2020) Biomedical x-ray imaging with a GaAs photon-counting detector: A comparative study. APL Photonics 5:106108
26. Zainon R, Ronaldson JP, Janmale T et al. (2012) Spectral CT of carotid atherosclerotic plaque: comparison with histology. Eur Radiol 22:2581–2588 [PubMed: 22760344]
27. Baer K, Kieser S, Schon B et al. (2021) Spectral CT imaging of human osteoarthritic cartilage via quantitative assessment of glycosaminoglycan content using multiple contrast agents. APL Bioeng 5:026101 [PubMed: 33834156]
28. Rajendran K, Löbker C, Schon BS et al. (2017) Quantitative imaging of excised osteoarthritic cartilage using spectral CT. Eur Radiol 27:384–392 [PubMed: 27165137]
29. Iwanczyk JS, Nygard E, Meirav O et al. (2009) Photon counting energy dispersive detector arrays for x-ray imaging. IEEE Transactions on Nuclear Science 56:535–542 [PubMed: 19920884]
30. Forghani R, De Man B, Gupta R (2017) Dual-Energy Computed Tomography Physical Principles, Approaches to Scanning, Usage, and Implementation: Part 1. Neuroimaging Clinics of North America 27:371-+ [PubMed: 28711199]
31. Arenson J (2009) Clinical Use of Photon Counting Detectors in CTAAPM 51st Annual Meeting. AAPM, Anaheim, California, USA
32. Romman Z (2009) Virtual Non-Contrast CT of the Abdomen Using a Dual Energy Photon Counting CT Scanner: Assessment of PerformanceRadiological Society of North America (RSNA) 95th Scientific Assembly and Annual Meeting. RSNA, Chicago, Illinois, USA
33. Kappler S, Glasser F, Janssen S, Kraft E, Reinwand M (2010) A research prototype system for quantum-counting clinical CTSPIE Medical Imaging. International Society for Optics and Photonics, pp 76221Z-76221Z–76226
34. Kappler S, Hahn K, Henning A et al. (2015) Towards High-Resolution Multi-Energy CT: Recent Results from our Whole-Body Prototype Scanner with High-flux Capable Photon Counting DetectorThe 3rd Workshop on medical applications of spectroscopic X-ray detectors CERN, Geneva, Switzerland

35. Kappler S, Hannemann T, Kraft E et al. (2012) First results from a hybrid prototype CT scanner for exploring benefits of quantum-counting in clinical CTSPIE Medical Imaging. International Society for Optics and Photonics, pp 83130X-83130X–83111
36. Kappler S, Henning A, Krauss B et al. (2013) Multi-energy performance of a research prototype CT scanner with small-pixel counting detectorSPIE Medical Imaging. International Society for Optics and Photonics, pp 86680O-86680O–86688
37. Kappler S, Henning A, Kreisler B, Schöeck F, Stierstorfer K, Flohr T (2014) Photon counting CT at elevated X-ray tube currents: contrast stability, image noise and multi-energy performanceSPIE Medical Imaging. International Society for Optics and Photonics, pp 90331C-90331C–90338
38. Leng S, Yu Z, Halaweish A et al. (2016) Dose-efficient ultrahigh-resolution scan mode using a photon counting detector computed tomography system. J Med Imaging 3:043504
39. Zhou W, Bartlett DJ, Diehn FE et al. (2019) Reduction of Metal Artifacts and Improvement in Dose Efficiency Using Photon-Counting Detector Computed Tomography and Tin Filtration. Invest Radiol 54:204–211 [PubMed: 30562270]
40. Rajendran K, Voss BA, Zhou W et al. (2020) Dose Reduction for Sinus and Temporal Bone Imaging Using Photon-Counting Detector CT With an Additional Tin Filter. Invest Radiol 55:91–100 [PubMed: 31770297]
41. Rajendran K, Petersilka M, Henning A et al. (2021) Full field-of-view, high-resolution, photon-counting detector CT: technical assessment and initial patient experience. Phys Med Biol 66
42. Rajendran K, Petersilka M, Henning A et al. (2022) First Clinical Photon-counting Detector CT System: Technical Evaluation. Radiology 303:130–138 [PubMed: 34904876]
43. Boccalini S, Si-Mohamed SA, Lacombe H et al. (2022) First in-human results of computed tomography angiography for coronary stent assessment with a spectral photon counting computed tomography. Investigative Radiology 57:212 [PubMed: 34711766]
44. Si-Mohamed SA, Boccalini S, Lacombe H et al. (2022) Coronary CT Angiography with Photon-counting CT: First-In-Human Results. Radiology 303:303–313 [PubMed: 35166583]
45. Si-Mohamed S, Boccalini S, Rodesch PA et al. (2021) Feasibility of lung imaging with a large field-of-view spectral photon-counting CT system. Diagn Interv Imaging 102:305–312 [PubMed: 33610503]
46. Schmidt TG (2009) Optimal “image-based” weighting for energy-resolved CT. Med Phys 36:3018–3027 [PubMed: 19673201]
47. Baek J, Pineda AR, Pelc NJ (2013) To bin or not to bin? The effect of CT system limiting resolution on noise and detectability. Phys Med Biol 58:1433–1446 [PubMed: 23399724]
48. Shikhaliev PM, Fritz SG, Chapman JW (2009) Photon counting multienergy x-ray imaging: effect of the characteristic x rays on detector performance. Med Phys 36:5107–5119 [PubMed: 19994521]
49. Taguchi K, Iwanczyk JS (2013) Vision 20/20: Single photon counting x-ray detectors in medical imaging. Med Phys 40:100901 [PubMed: 24089889]
50. Ballabriga R, Campbell M, Heijne EHM, Llopart X, Tlustos L (2007) The medipix3 prototype, a pixel readout chip working in single photon counting mode with improved spectrometric performance. IEEE Transactions on Nuclear Science 54:1824–1829
51. Koenig T, Zuber M, Hamann E et al. (2014) How spectroscopic x-ray imaging benefits from inter-pixel communication. Phys Med Biol 59:6195–6213 [PubMed: 25255737]
52. Hsieh SS (2020) Coincidence Counters for Charge Sharing Compensation in Spectroscopic Photon Counting Detectors. IEEE Trans Med Imaging 39:678–687 [PubMed: 31398114]
53. Hsieh SS, Sjolin M (2018) Digital count summing vs analog charge summing for photon counting detectors: A performance simulation study. Med Phys 45:4085–4093

Key points:

1. Energy resolving, photon-counting-detector CT is an important advance in CT technology.
2. Relative to current energy-integrating scintillating detectors, energy resolving, photon-counting-detector CT offers improved spatial resolution, improved contrast-to-noise ratio, elimination of electronic noise, increased radiation and iodine dose efficiency, and simultaneous multi-energy imaging.
3. High-spatial-resolution, multi-energy imaging using energy resolving, photon-counting-detector CT has been used in investigations into new imaging approaches, including multi-contrast imaging.

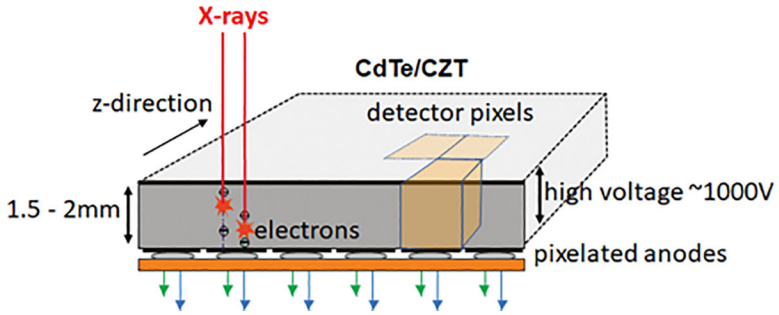

Figure 1:

Schematic representation of a photon counting detector. The z-direction is the patient's longitudinal direction. The detector pixels (three pixels are schematically indicated) are virtually formed by the pixelated anodes and the strong electric field, without the use of physical septa to separate the pixels. The pixels can be very small (e.g., 0.15×0.18 mm^2 when projected onto the isocentre of the scanner).

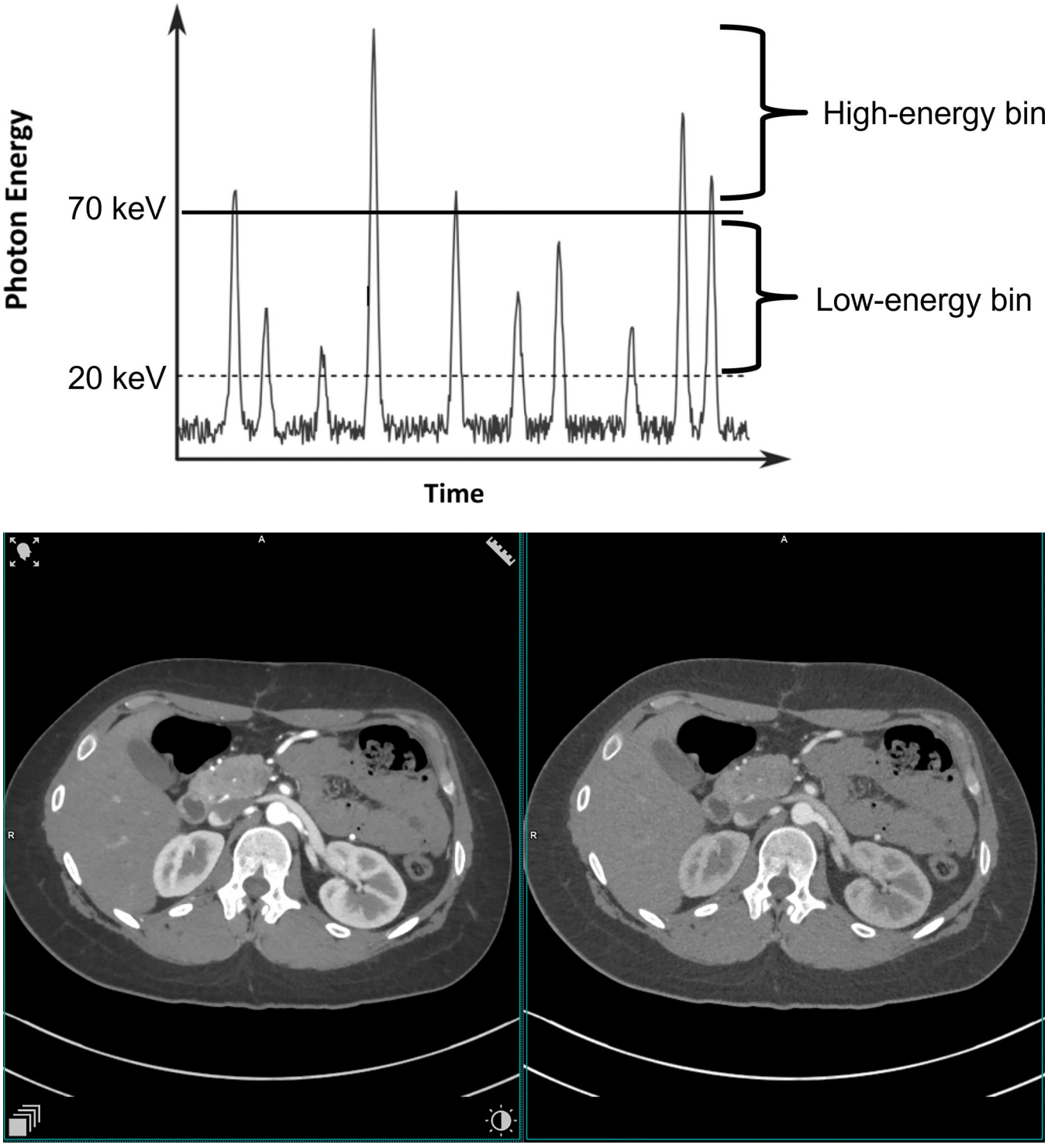

Figure 2:

Top - Schematic illustration of data acquisition at two threshold energies (T_{LOW} = 20 keV, T_{HIGH} = 70 keV) providing two spectrally resolved detector signals. Bottom - Contrast-enhanced abdominal scan of a 25-year-old female acquired with a clinical photon counting CT prototype with two threshold energies as indicated above.

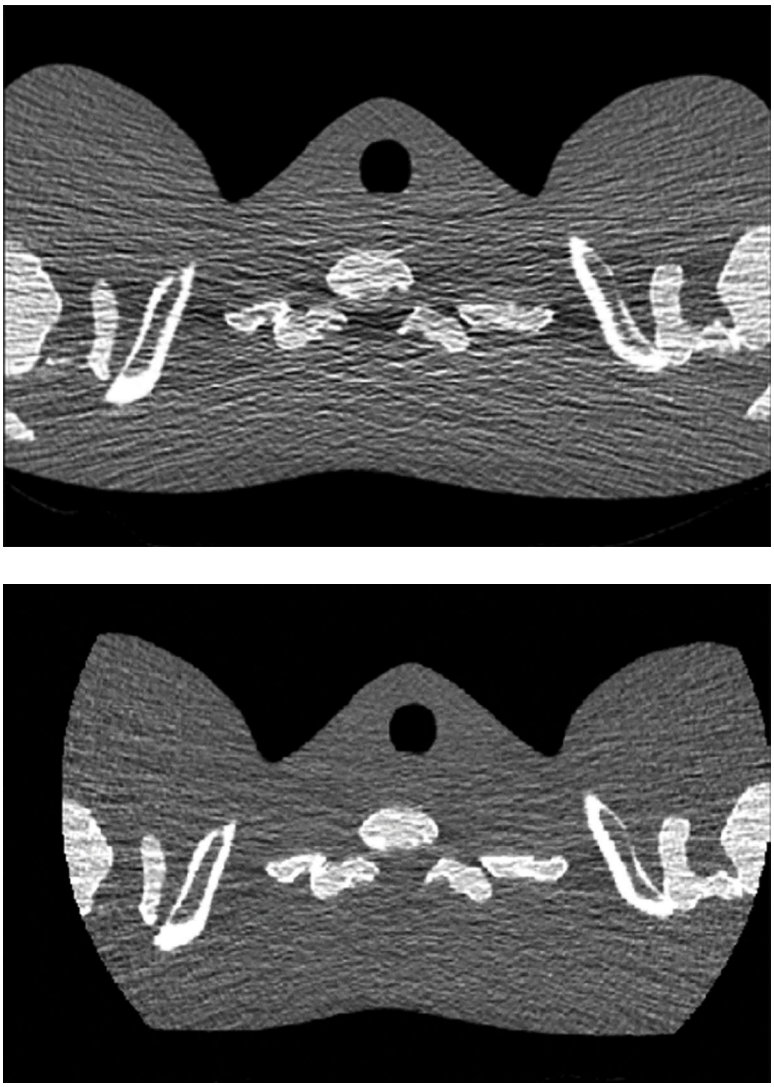

Figure 3:
Images of an anthropomorphic shoulder phantom from an EID (A) and a PCD (B) at low photon flux. The PCD images have noticeably less horizontal streak artifacts and an overall more uniform appearance than the EID image. Beam hardening artifacts (dark banding) were present in both images. Display W/L=900/40 HU [EID: energy integrating detector; PCD: photon-counting-detector]. Images reproduced with permission from [7].

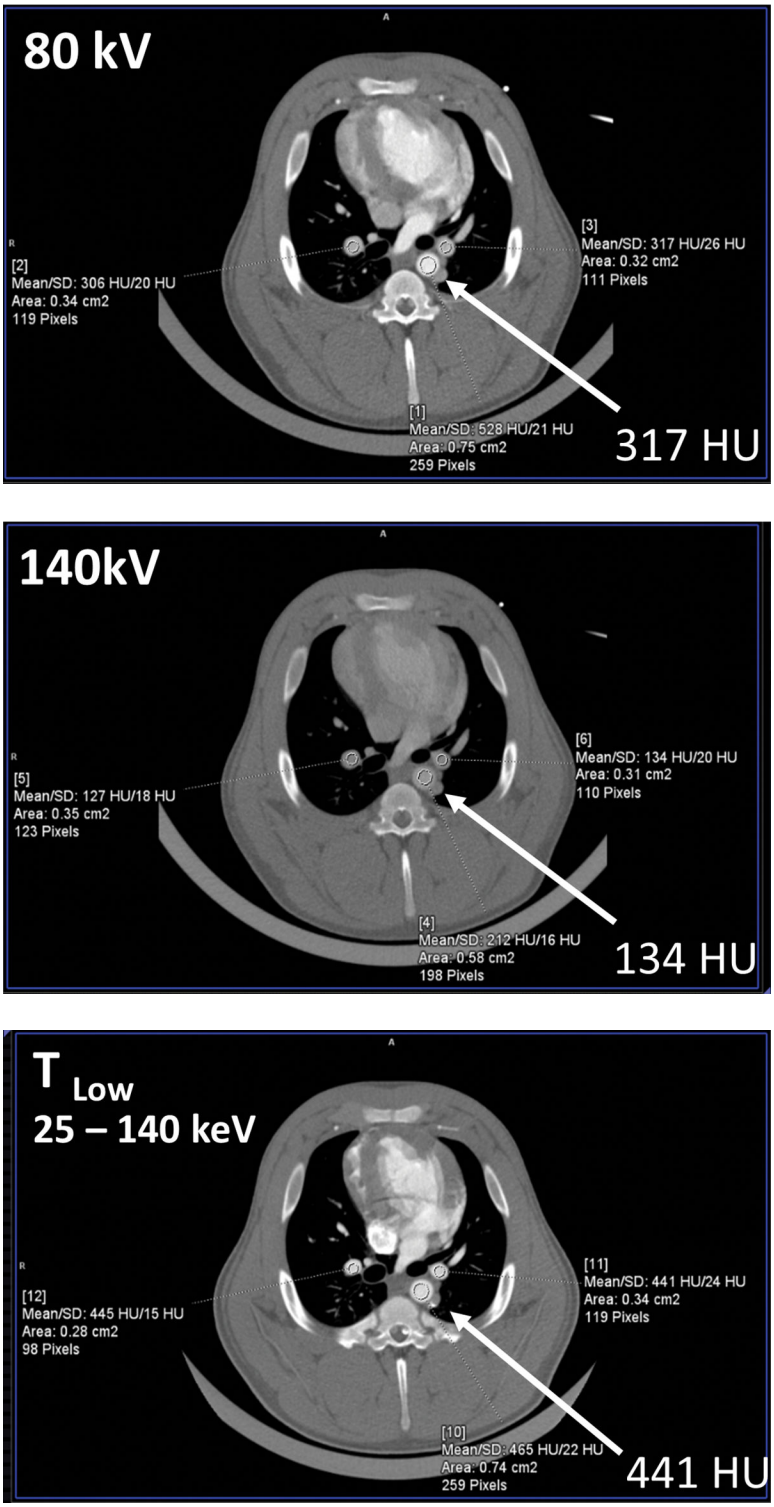

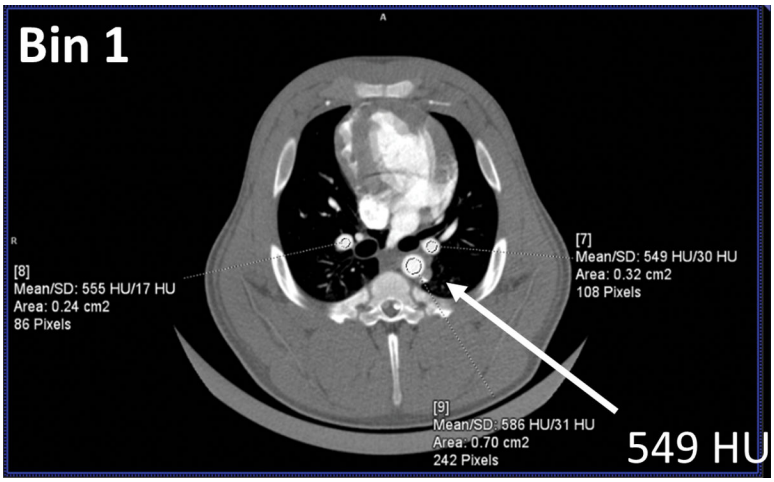

Figure 4:

Top - EID-CT images of a swine scanned at 80 and 140 kV demonstrate the strong decrease in iodine contrast at the higher tube potential. Bottom - PCD-CT images of the same animal scanned at 140 kV. The iodine signal in the aorta (arrows) is higher for the low-energy threshold image (T_{Low}), which contains photons from 25–140 keV. The Bin 1 image, which contains photons from 25–65 keV, has the highest iodine signal, even brighter than that obtained at 80 kV on an EID-CT system. [EID: energy integrating detector; PCD: photon-counting-detector]

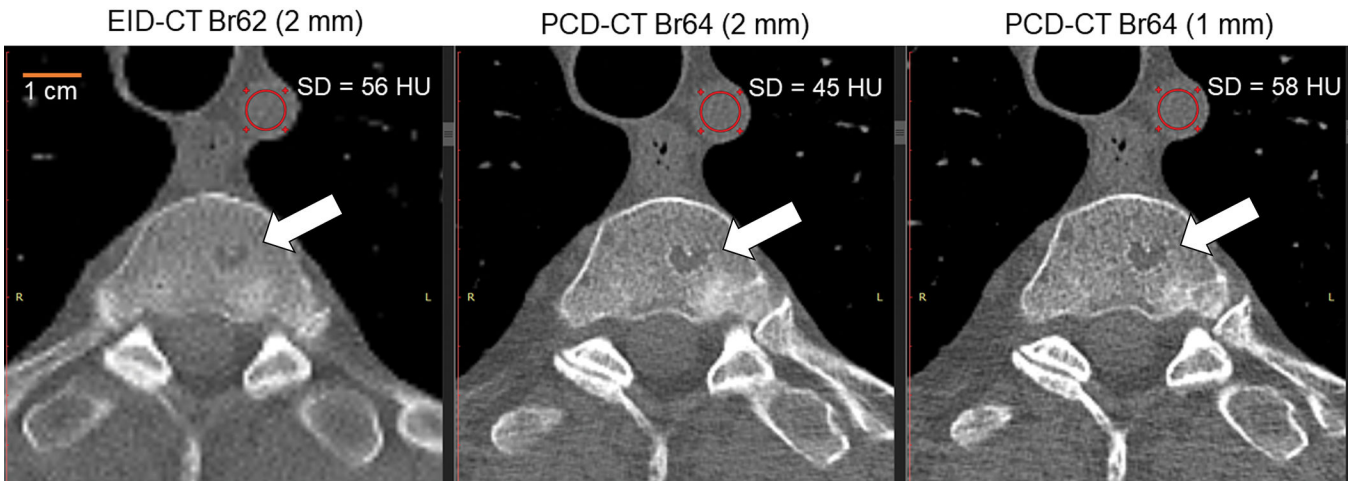

Figure 5:

Axial images of a 74-year-old man from a clinically indicated whole-body low-dose CT skeletal survey for multiple myeloma. EID-CT image (left) and high-spatial-resolution photon-counting detector PCD-CT images (center and right) were acquired using the same radiation dose (4.2 mGy), slice thickness (2 mm), and nearly identical reconstruction kernels (B62 and B64), and matric size (512). The PCD-CT 2-mm image (center) showed 20% lower noise (56 HU vs 45 HU within the white circular regions of interest) relative to the otherwise matched EID-CT image (left). This is a consequence of the inherently higher intrinsic resolution of the PCD system. Use of thinner (1 mm) slice thickness (right) and 1024 × 1024 matrix resulted in improved spatial resolution but with image noise similar to that of the EID-CT image. Improved delineation of a vertebral lesion (arrows) can be appreciated. Thus, compared to an EID-CT, the improved resolution of the PCD-CT may not require an increase in patient dose to achieve the same image noise level. Display window = 1500 HU; display level = 150 HU. Br = body-regular reconstruction kernel, SD = standard deviation of pixel values in region of interest. [EID: energy integrating detector; PCD: photon-counting-detector].

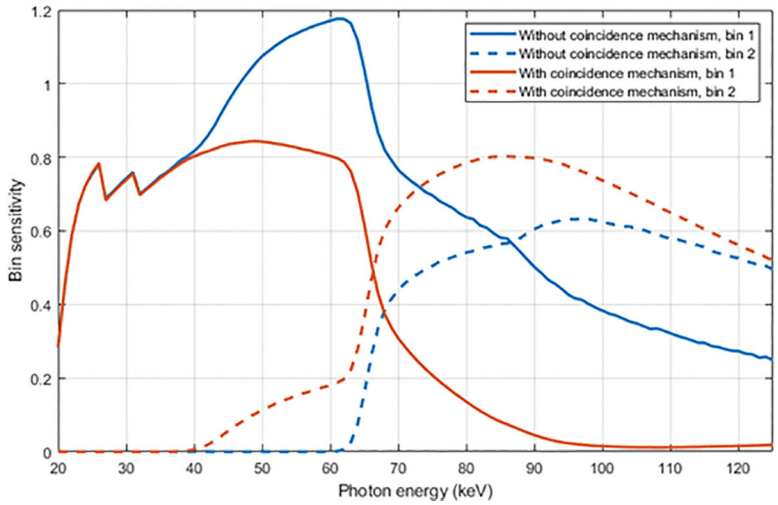

Figure 6:

Bin sensitivities (counts per incoming photon) as a function of input photon energy for CdTe photon counting detectors, pixel size 300 μm, thresholds 20 and 65 keV. The blue lines show the sensitivities without any coincidence counting mechanisms. The brown lines show the response for a detector including a simple coincidence counting mechanism where two counts in the lower energy bin in two neighbouring pixels are replaced by one count in the upper energy bin in one of the pixels.